Mutations at Positions 153 and 328 inEscherichia coliAlkaline Phosphatase Provide Insight Towards the Structure and Function of Mammalian and Yeast Alkaline Phosphatases

ARTICLE *in* JOURNAL OF MOLECULAR BIOLOGY · DECEMBER 1995

Impact Factor: 4.33 · DOI: 10.1006/jmbi.1995.0576 · Source: PubMed

3 AUTHORS, INCLUDING:

Thomas T Tibbitts
Infinity Pharmaceuticals
11 PUBLICATIONS **357** CITATIONS

J. Mol. Biol. (1995) **253**, 604–617

JMB

Mutations at Positions 153 and 328 in *Escherichia coli* Alkaline Phosphatase Provide Insight Towards the Structure and Function of Mammalian and Yeast Alkaline Phosphatases

Jennifer E. Murphy, Thomas T. Tibbitts and Evan R. Kantrowitz*

Boston College, Department of Chemistry, Merkert Chemistry Center, Chestnut Hill MA 02167-3860, USA

**Corresponding author*

In order to understand some of the differences between human placental, human, *Saccharomyces cerevisiae* and *Escherichia coli* alkaline phosphatases in specific activity, activation by magnesium, and pH *versus* activity profiles, the X-ray crystal structures of three mutant *E. coli* alkaline phosphatases have been determined. The aligned sequences of alkaline phosphatases from mammalian, yeast and *E. coli* show that 25 to 30% of the amino acids are absolutely conserved and the active site residues are completely conserved with the exception of residues 153, 328 and 155. The bacterial enzyme has a salt-bridge, Asp153/Lys328, near the third metal binding site which, based on sequence homology, is apparently absent in the yeast and mammalian enzymes. The human enzymes have histidine at positions 153 and 328, and the yeast enzyme has histidine at position 328. In the *E. coli* enzyme, Asp153 was replaced by histidine (D153H), Lys328 was replaced by histidine (K328H), and a double mutant (DM) was constructed containing both mutations. The structure of the K328H enzyme was refined using cross-validation to a resolution of 2.3 Å with a working *R*-factor of 0.181 and a free *R*-factor of 0.249. The DM structure was determined to a resolution of 2.5 Å with a working *R*-factor of 0.166 and a free *R*-factor of 0.233. The structure of the D135H enzyme, which has been reported to a resolution of 2.4 Å, has been re-refined using cross-validation to a working *R*-factor of 0.179 and a free *R*-factor of 0.239 for controlled comparisons with the two new structures. In all three structures the most significant changes are related to the bound phosphate inhibitor and the identity of the metal ion in the third binding site. The changes in the position of the phosphate group and the alterations at the third metal binding site indicate the structural basis for the variations in the steady-state kinetic parameters previously reported for these enzymes.

Keywords: X-ray diffraction; metalloenzymes; protein structure-function; site-specific mutagenesis; cross-validation

Introduction

Sequence determinations have shown that alkaline phosphatase has been highly conserved during evolution. The amino acid sequence of alkaline phosphatase from *Escherichia coli* (Bradshaw *et al*., 1981), human placenta (Kam *et al*., 1985), human b/k/l (Weiss *et al*., 1986), human intestine (Berger *et al*., 1987) and *Saccharomyces cerevisiae* (Kaneko *et al*., 1987) have been determined directly, or have been deduced from the corresponding cDNA sequences. Comparison of the mammalian and yeast alkaline phosphatases with the *E. coli* alkaline phosphatase has shown that the amino acid sequence is 25 to 30% absolutely conserved. The active sites of the human, yeast, and *E. coli* alkaline phosphatases are completely conserved, with three

Abbreviations used: D153H, the *E. coli* mutant alkaline phosphatase in which Asp153 has been replaced by histidine; K328H, the mutant *E. coli* alkaline phosphatase in which Lys328 has been replaced by histidine; DM, the mutant *E. coli* alkaline phosphatase in which both Asp153 and Lys328 have been replaced by histidine. The abbreviation b/k/l represents bone/kidney/liver and is used when referring to the tissue non-specific human alkaline phosphatases.

0022–2836/95/440604–14 $12.00/0

Table 1. Conservation of the metal ligands in alkaline phosphatases from different species at positons 153 and 328

	Metal ligands in the *E. coli* enzyme										
	M1			M2			M3				
Species	327	331	412	370	369	51	322	155	**153**	**328**	Reference
E. coli wild-type	Asp	His	His	His	Asp	Asp	Glu	Thr	**Asp**	**Lys**	Bradshaw *et al*. (1981)
E. coli D153H	Asp	His	His	His	Asp	Asp	Glu	Thr	**His**	**Lys**	Janeway *et al*. (1993)
E. coli K328H	Asp	His	His	His	Asp	Asp	Glu	Thr	**Asp**	**His**	Xu & Kantrowitz (1991)
S. cerevisiae	Asp	His	His	His	Asp	Asp	Glu	Thr	**Asp**	**His**	Kaneko *et al*. (1987)
E. coli DM	Asp	His	His	His	Asp	Asp	Glu	Thr	**His**	**His**	Janeway *et al*. (1993)
Human b/k/l	Asp	His	His	His	Asp	Asp	Glu	Thr	**His**	**His**	Weiss *et al*. (1986)
Human intestinal	Asp	His	His	His	Asp	Asp	Glu	Ser	**His**	**His**	Berger *et al*. (1987)
Human placental	Asp	His	His	His	Asp	Asp	Glu	Ser	**His**	**His**	Kam *et al*. (1985)

exceptions. Positions 153 and 328 in the three human enzymes (numbering of the residues in the mammalian and yeast enzymes is based on homology to the *E. coli* enzyme) are invariably histidine while they are aspartate and lysine, respectively, in the *E. coli* enzyme (Table 1). In the yeast enzyme, position 328 is histidine, although position 153 is aspartate as in the *E. coli* enzyme. The only other difference between the active site residues is a conservative substitution at position 155. In the *E. coli* and the human b/k/l enzymes this position is occupied by threonine, while in the yeast and human placental enzymes position 155 is occupied by serine.

There are important functional differences between human, yeast and *E. coli* alkaline phosphatases; the mammalian enzymes are ten- to 20-fold more active than the bacterial enzyme, much less heat stable, and exhibit a shift in the pH *versus* activity profile towards higher pH. In addition, some mammalian alkaline phosphatases require magnesium in order to achieve maximum activity (Brunel & Cathala, 1973; Cathala *et al*., 1975; and see Table 2). The non-specific alkaline phosphatase found in yeast also requires magnesium for maximum activity, and its pH *versus* activity profile is also shifted towards more alkaline pH (Schurr & Yagil, 1971). Although the catalytic mechanism of the human and yeast enzymes is not known, it is presumed to be similar to that of the *E. coli* enzyme, since the active site residues are so highly conserved.

E. coli alkaline phosphatase (EC 3.1.3.1) functions as a nonspecific phosphomonoesterase that proceeds through a phosphoseryl intermediate (Schwartz & Lipmann, 1961) to produce inorganic phosphate and an alcohol. The catalytic mechanism has been the subject of many kinetic (Coleman, 1992) and structural studies (Kim & Wyckoff, 1991). Two zinc atoms play a direct role in the catalytic mechanism of the *E. coli* enzyme (Kim & Wyckoff, 1991). Though magnesium does not appear to be directly involved in catalysis, it has been shown to be important for full activation of the enzyme (Anderson *et al*., 1975, 1976). The rate determining step of the mechanism is pH dependent; at acidic pH the hydrolysis of the covalent enzyme-phosphate complex (E-P_i) is rate-limiting, while under basic conditions the rate-limiting step becomes the release of phosphate from the non-covalent enzyme-phosphate complex (E·P_i; Bloch & Gorby, 1980; Gettins & Coleman, 1983; Hull *et al*., 1976; Reid & Wilson, 1971).

The X-ray structure of the *E. coli* enzyme was first solved by Sowadski *et al*. (1983, 1985) to 2.8 Å and later it was further refined to 2.0 Å resolution (Kim & Wyckoff, 1991). The alkaline phosphatase structure consists of a dimer containing two atoms of zinc and one atom of magnesium per monomer with the inhibitor inorganic phosphate bound between the two zinc atoms in each active site (Figure 1). Phosphate is held tightly in the active site, providing oxygen ligands to the two zinc atoms, charged hydrogen bonds to the guanidino nitrogen atoms of Arg166, and a water-mediated interaction with Lys328, which has been shown to be important for binding of the phosphate (Xu & Kantrowitz, 1991;

Table 2. Kinetic parameters of the *E. coli*, yeast and mammalian enzymes at optimal pH

Enzyme	pH	Mg^{2+} activated	V_{max} (μmol min^{-1} mg^{-1})	K_m (mM)	K_i (mM)	Reference
E. coli wild-type	8.0	—[a]	57	0.02	0.045	Janeway *et al*. (1993)
D153H	10.5	+[b]	185	0.54	0.033	Janeway *et al*. (1993)
K328H	10.3	—	159	1.4	0.33	Janeway *et al*. (1993)
S. cerevisiae	8.9	+	na[c]	0.45	0.70[d]	Schurr & Yagil (1971)
DM	9.5	+	324	0.61	1.30	Janeway *et al*. (1993)
Human b/k/l	10.0	+	790	0.36	na	Cathala *et al*. (1975)
Human intestinal	9.8	—	3920	na	na	Hua *et al*. (1986)
Human placental	10.5	—	760	0.80	na	Harkness (1968)

[a] After purification additional magnesium does not activate the enzyme further.
[b] After purification additional magnesium activates the enzyme further.
[c] Not available.
[d] Estimated value based on kinetic data from Schurr & Yagil (1971).

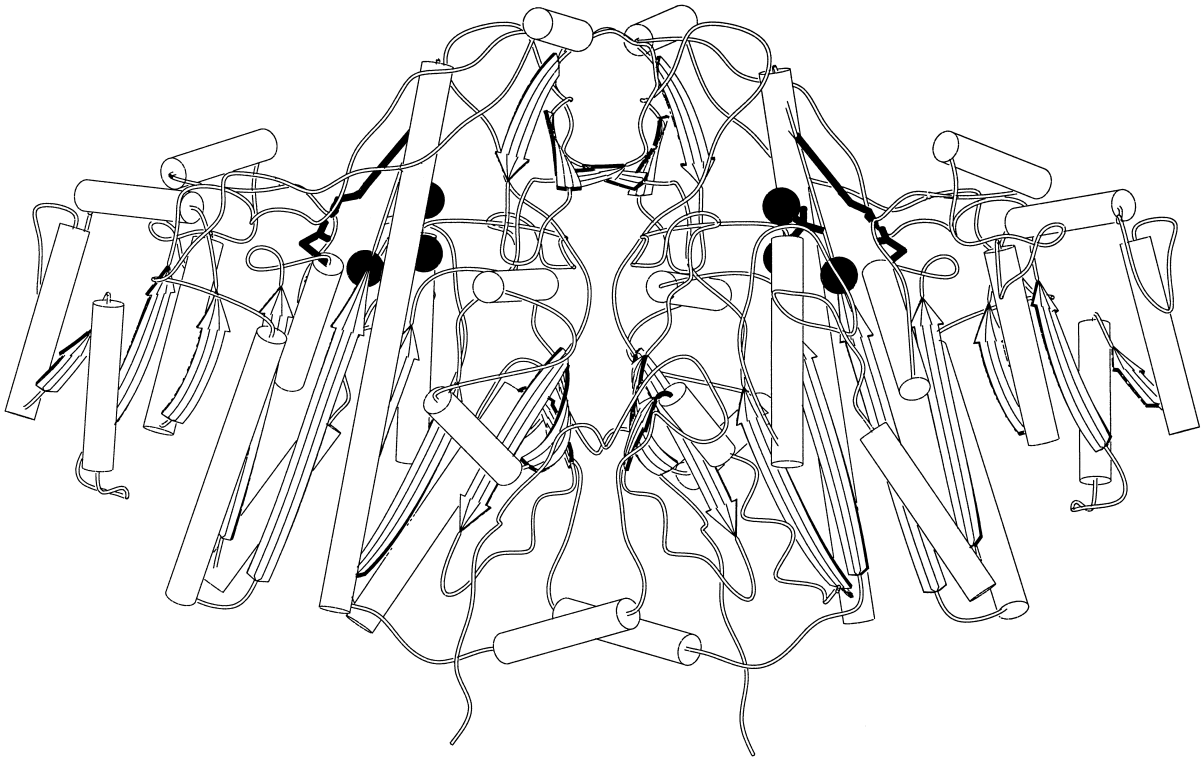

Figure 1. Schematic representation of the secondary structure of the alkaline phosphatase dimer based on the X-ray crystallographic data of Kim & Wyckoff (1991). The β-sheets are shown as ribbons with arrows denoting the direction; the α-helices are shown as tubes. The six metal binding sites are designated by filled spheres. The phosphate group can be seen in the active site of the A chain (right-hand side) while the side-chains of Lys328 and Asp153 are highlighted in each of the monomers. The phosphate group cannot be seen in the B chain (left-hand side), since it is behind an α-helix.

and see Figure 2). Magnesium is coordinated octahedrally by three water molecules, the carboxylate oxygens of Asp51 and Glu322, and the hydroxyl group of Thr155. Asp153 interacts indirectly with magnesium through two of the three water molecules, and has been shown to be important for magnesium binding (Janeway *et al*., 1993; Murphy & Kantrowitz, 1994; Murphy *et al*., 1993).

In order to evaluate the functional differences between human, yeast and *E. coli* alkaline phosphatases, mutations in the *E. coli* enzyme were made at positions 153 and 328 using site-directed mutagenesis. Two single mutants, D153H and K328H, and a double mutant, DM, were constructed and characterized kinetically (Janeway *et al*., 1993; Xu & Kantrowitz, 1991; and see Table 2). These enzymes exhibited many of the properties of the mammalian enzymes, including low activity in the absence of magnesium, enhanced activity induced in a time-dependent fashion by magnesium, and a shift in the pH of optimal activity. The X-ray structure of the D153H enzyme, determined to 2.4 Å resolution, showed that the replacement of Asp153 by histidine changed the metal at the M3 site† from an octahedrally coordinated magnesium, seen in the wild-type structure, to a tetrahedrally coordinated zinc (Murphy & Kantrowitz, 1994; Murphy *et al*., 1993), demonstrating that it is possible to alter the metal specificity of an enzyme by a single amino acid substitution. A change in the metal occupying the third metal binding site also provided a possible explanation for the magnesium activation of certain mammalian alkaline phosphatases.

In this study, further X-ray crystallographic analysis was undertaken to explain the kinetic behavior of

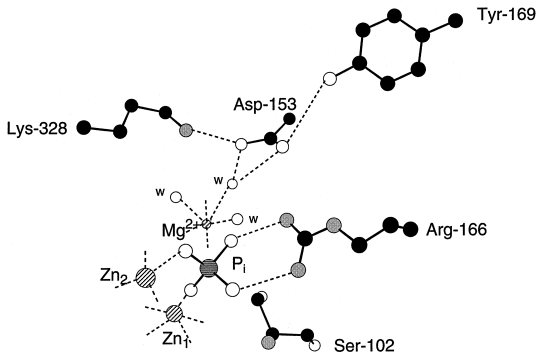

Figure 2. The active site region of *E. coli* alkaline phosphatase including the phosphate group, magnesium ion and two zinc-binding sites. Not all the ligands are shown. Water molecules are indicated by the letter w. Hydrogen bonds are shown as broken lines (Kim & Wyckoff, 1991).

† The Zn_1, Zn_2 and Mg metal sites correspond to the M1, M2 and M3 sites, respectively, identified by X-ray crystallography of the wild-type enzyme (Sowadski *et al*., 1983).

Table 3. Data collection summary of the D153H, K328H and DM alkaline phosphatases

Enzyme	Space group	d_{min} (Å)	Reflections total / unique	Completness (%)	Redundancy	Unit cell[a] (Å)	Final R_{merge}
D153H	*I*222	2.4	194,028 47,928	98	4.0	*a* = 194.77 *b* = 166.96 *c* = 76.33	0.090
K328H	*I*222	2.3	214,198 55,520	99	3.9	*a* = 195.1 *b* = 167.3 *c* = 76.5	0.080
DM	*I*222	2.5	118,201 39,775	91	3.0	*a* = 194.6 *b* = 167.3 *c* = 76.3	0.072

[a] Unit cell dimensions of the wild-type enzyme: *a* = 195.3 Å, *b* = 167.4 Å, *c* = 76.2 Å.

the engineered bacterial enzymes, and to visualize the structural consequences of introducing histidine at positions 153 and 328. The D153H, K328H and DM enzymes have been crystallized and their structures determined to 2.4 Å, 2.3 Å and 2.5 Å, respectively. The refined structures are presented here along with a comparison, particularly in the active site region, of the K328H, D153H, DM and the wild-type structures.

Results

Crystallization and data collection

The space group of the D153H, K328H and DM crystals was *I*222, identical with that of the wild-type enzyme (Kim & Wyckoff, 1991). Statistics from the data collections are summarized in Table 3. The unit cell dimensions did not differ substantially from those of the wild-type or other *E. coli* alkaline phosphatase X-ray structures previously reported (Kim & Wyckoff, 1991; Chen *et al.*, 1992; Ma *et al*., 1995; Murphy *et al*., 1993; Tibbitts *et al*., 1994).

Refinement

The wild-type coordinates were used as the initial model for each of the structure refinements using X-PLOR (Brünger, 1992b) with cross-validation testing (Brünger, 1992a) and the Engh & Huber (1991) chemical parameters. Initially, the metal ions and the phosphate group were removed from the two active sites and water molecules were not included in the refinement. The working *R*-factor, calculated for 90% of the reflections and the free *R*-factor, calculated for the other 10% of reflections not included in the refinement, were set up in the beginning, and followed during each stage of the refinement. The first refinement procedure was a simulated annealing in order to decouple the working and free *R*-factors (Brünger *et al*., 1990). After several rounds of refinement, the metal ions and the phosphate group were built into the density observed in simulated annealing omit density maps (Hodel, 1992) calculated for the two active sites. The beginning free *R*-factors for the D153H, K328H and DM structures were 0.269, 0.267 and 0.350, respectively, while the initial working *R*-factors were 0.240, 0.232 and 0.352, respectively. The models were further refined through cycles of positional refinement, temperature factor refinement, automatic water addition (described below), and rigid body refinement using non-crystallographic symmetry restraints (Tibbitts *et al*., 1994), bringing the free *R*-factor values for the D153H, K328H and DM structures down to 0.239, 0.249 and 0.233, respectively, while the final working

Table 4. Refinement statistics for the D153H, K328H and DM alkaline phosphatase structures

Enzyme form	Final *R*-factor[a]	Working *R*-factor beginning end	Free *R*-factor beginning end	Water molecule	Water sigma[b]	RMS deviations: Bond lengths (Å)	Bond angles (deg.)	Improper / dihedral angles (deg.)
D153H	0.185	0.240 0.179	0.269 0.239	186	3.7	0.016	1.83	24.2 / 1.70
K328H	0.194	0.232 0.181	0.267 0.249	318	3.2	0.020	2.00	24.2 / 1.97
DM	0.176	0.352 0.166	0.350 0.233	270	3.1	0.019	1.98	24.7 / 1.84

[a] The use of cross-validation with one free *R*-factor (Brünger, 1993) involves partitioning of the observed intensities in two disjoint subsets, placing a small percentage (10%) in a test set *T* and the remainder in a working set *A*. The choice of which reflections *hkl* go into the test set is done by random selection. The reflections placed in the test set are not used in refinement by procedures in X-PLOR. The X-PLOR energy function is minimized with only the reflections from the set *A* included. After each refinement step, values for the working *R*-factor *R*(*A*) and free *R*-factor *R*(*T*) are calculated. If the *R*-factor *R*(*T*) decreases, the refinement step is accepted. If the *R*(*T*) increases, the refinement step is rejected. If the *R*(*T*) remains constant then the refinement step is evaluated based on the working *R*-factor *R*(*A*). If *R*(*A*) decreases, the refinement step is rejected, and if *R*(*A*) increases or remains constant the refinement step is accepted.
[b] Contour level in the $F_o - F_c$ density maps used to identify peaks for water placement.

R-factors were 0.179, 0.181 and 0.166 respectively (Table 4).

At each stage of the refinement, water molecules were automatically added using IMPLOR (T.T.T., unpublished) at positions indicated by their density in omit maps ($F_o - F_c$). Temperature factors of the solvent molecules were closely monitored during refinement. The water molecules were tested automatically by IMPLOR for high temperature factors and hydrogen-bonding distances. Coordinates of the water molecules with temperature factors greater than 59 Å^2 were deleted from the model, and checked against the omit density after the next refinement cycle. Any water molecule that did not pass the testing requirements was eliminated. At the end of the refinement 186 water molecules were added to the D153H structure, 318 to the K328H structure and 270 to the DM structure (Table 4). At this point the working and test sets were recombined and a short refinement performed with all the data, which did not appreciably alter the models. The final *R*-factors are reported in Table 4.

Refinement was considered complete when each of the available procedures, including water building, failed to further reduce the free *R*-factor.

Geometrical and stereochemical analysis

The average root-mean-square deviation (RMSD) of the α-carbon and side-chain positions between the mutant and the wild-type structures were calculated. The average RMSD values for the D153H, K328H and DM structures were 0.20 Å, 0.33 Å and 0.18 Å, respectively for the α-carbon atoms, and 0.50 Å, 0.62 Å and 0.50 Å, respectively for the side-chains. These comparisons showed that, overall, the three mutant structures did not differ substantially from the structure of the wild-type enzyme.

The geometrical analysis shows that the values in Table 4 are reasonable for Engh & Huber parameters (Brändén & Jones, 1990). The W_A value was calculated based on the minimum free *R*-value using simulated annealing calculations, and was set to 3.0×10^6 for each of the structures.

Ramachandran plots of the phi-psi angles for the final refined coordinates for the D153H, K328H, and DM enzymes indicated that nearly all the residues were in the most favored regions (Figure 3). The uncertainty in the refined coordinates for the D153H, K328H and DM structures was estimated to be ± 0.25, ± 0.275 and ± 0.25, respectively, from Luzzati plots showing the resolution dependence of the *R*-factors (Figure 4).

Comparison between the wild-type and mutant structures

Active site of the D153H structure

The active site in the D153H structure refined using the Engh & Huber (1991) parameters is nearly indistinguishable from the earlier refinement (Murphy *et al*., 1993) using the Brooks parameters (Brooks *et al*., 1983) to within the estimated uncertainty; however, additional water molecules have been added and tested (Table 4). The salt-link between Asp153 and Lys328, present in the wild-type structure, did not form between histidine and lysine side-chains in the D153H enzyme. Instead, the side-chain of His153 became a direct ligand to the metal ion, at the M3 site. In the mutant enzyme, Lys328 directly interacts with the phosphate group, providing a new charged hydrogen bond, which is consistent with its increased affinity for phosphate (Janeway *et al*., 1993). The phosphate group in the D153H structure is coordinated to both Zn_1 and Zn_2 through one of its oxygen atoms, and Ser102 is directly interacting with Zn_2. The distance between Zn_2 and the hydroxyl of Ser102 is 2.1 Å in the D153H structure and 3.9 Å in the wild-type structure (Table 5). The metal ion at the M3 site in the D153H structure was modeled as zinc based on the strong scattering density at the M3 site and the previously reported structural results (Murphy *et al*., 1993).

A new anion binding site (PO_4-B) was observed in the active site of the D153H structure that had not been recognized previously. In the crystal, this site could be occupied by either a phosphate or sulfate group. The anion is hydrogen-bonded by the hydroxyl group of Tyr169, the NE nitrogen atom of Arg166, the ND2 nitrogen atom of His153, as well as two bound water molecules. A phosphate group was modeled into the A chain and its occupancy refined to 0.78, while the density corresponding to this anion in the B chain was not apparent, and thus the anion is not included in the model coordinates.

The active site of the K328H structure

Analysis of $2F_o - F_c$, $F_o - F_c$ and simulated annealing omit maps indicated that the K328H structure differed significantly from the wild-type structure at the active site (Figure 5). The replacement of Lys328 by histidine resulted in a displacement of the phosphate, and the loss of the salt-link that normally exists between Lys328 and Asp153 in the wild-type structure. Furthermore, the maps independently confirmed the mutation. In the K328H structure, the flattened, ellipsoidal shape of the density indicated that the side-chain at position 328 was due to an imidazole ring rather than an extended hydrocarbon chain characteristic of a lysine. The ND1 atom of His328 was located 2.7 Å away from the hydroxyl group of Ser325, close enough to form a hydrogen bond. The average temperature factor of His328 in the K328H structure was 35 Å^2 compared with 6 Å^2 for Lys328 in the wild-type structure. Asp153 shifted by 0.8 Å from its position in the wild-type, closer to the M3 site, had an average temperature factor of 17 Å^2, and was located 3.2 Å from the metal ion at the M3 site in the K328H structure. The metal-ligand distances are summarized in Table 5.

The metal sites at all three positions in the K328H structure were fully occupied. Initially, it was not clear whether the metal ion in the M3 position was zinc or magnesium. From the density distribution in

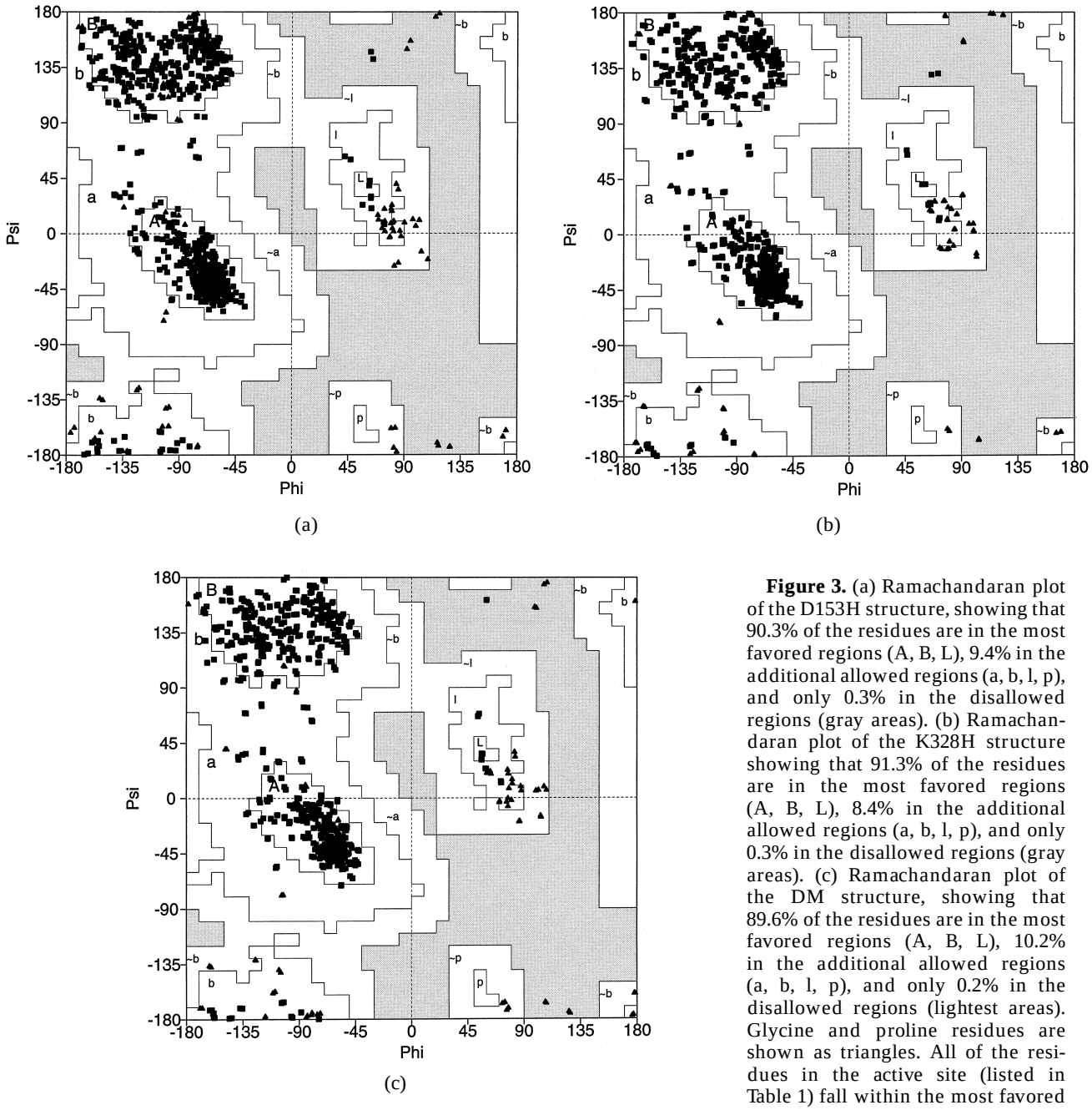

Figure 3. (a) Ramachandaran plot of the D153H structure, showing that 90.3% of the residues are in the most favored regions (A, B, L), 9.4% in the additional allowed regions (a, b, l, p), and only 0.3% in the disallowed regions (gray areas). (b) Ramachandaran plot of the K328H structure showing that 91.3% of the residues are in the most favored regions (A, B, L), 8.4% in the additional allowed regions (a, b, l, p), and only 0.3% in the disallowed regions (gray areas). (c) Ramachandaran plot of the DM structure, showing that 89.6% of the residues are in the most favored regions (A, B, L), 10.2% in the additional allowed regions (a, b, l, p), and only 0.2% in the disallowed regions (lightest areas). Glycine and proline residues are shown as triangles. All of the residues in the active site (listed in Table 1) fall within the most favored regions of the plots. The non-Pro and non-Gly outlier shown in the plots is Asn293 from the A and B chains. lt is not in the vicinity of the active site. These Figures were drawn using PROCHECK (Laskowski *et al*., 1993).

the simulated annealing omit maps the metal ion at the M3 site in the A chain appeared to be coordinated by Thr155, Asp51, Glu322 and three water molecules. This approximately octahedral geometry at the M3 site suggested that the metal was magnesium; however, when magnesium was modeled into this position the temperature factor refined to the minimum allowed value of 2 Å^2, indicating additional scattering density was needed. When zinc was modeled in the M3 site, the temperature factor refined to a reasonable value of 25 Å^2. The coordination around the M3 site in the B chain was somewhat different. The M3 position appeared to have only three ligands, Thr155, Glu322 and Asp51. Furthermore, there was no density unaccounted for in the $F_o - F_c$ map surrounding the M3 site, indicating that if there were some water molecules coordinated to the metal at that site they had very low occupancy. Zinc was therefore modeled into the M3 site in the B chain and the *B*-factor refined to 31 Å^2. With the three zinc atoms omitted, the difference density corresponding to the M3 site was nearly identical in shape and size with the density observed in the M1 and M2 sites, providing additional evidence that zinc occupied the M3 site. Therefore, we concluded that the K328H structure contained zinc at all six metal sites.

The coordination of Zn_1 and Zn_2 in the K328H

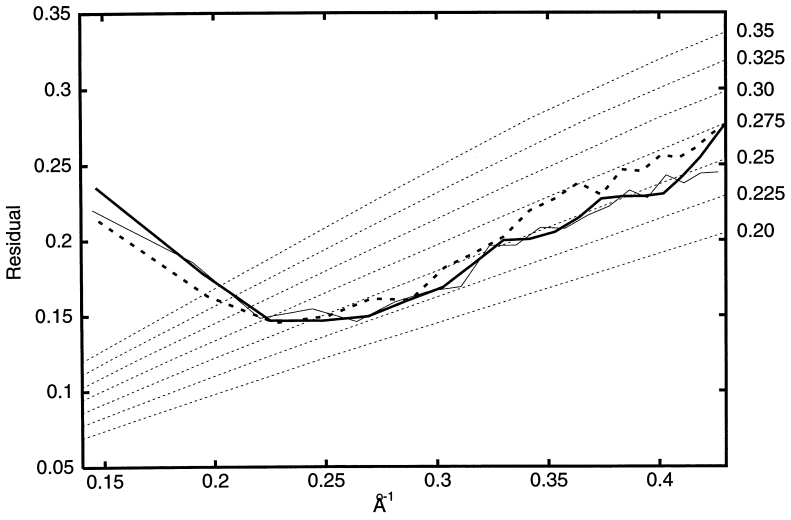

Figure 4. Luzzati plot (Luzzati, 1952) showing the final *R*-factors, by resolution shell, for the D153H, K328H, and DM structures. The thickest continuous line corresponds to the D153H structure, the broken line represents the K328H structure, and the thin continuous line represents the DM structure.

structure showed significant differences from the wild-type structure. Zn_1 was coordinated to the NE2 nitrogen atoms of His412 and His331, the OD1 and OD2 oxygen atoms of Asp327, and the O2 oxygen atom of the phosphate group. This is similar to the Zn_1 coordination in the wild-type structure. The hydroxyl oxygen atom of Ser102 interacts directly with Zn_2, as indicated by continuous density between the two atoms and a distance of 1.9 Å (Figure 5). In the wild-type structure, the phosphate group is coordinated to Zn_2 and the Ser102 hydroxyl group apparently points away from the metal (Kim & Wyckoff, 1991).

The phosphate group, normally coordinated by both Zn_1 and Zn_2 in the wild-type structure, moved 2 Å away from the active site pocket, towards the solvent (Figure 6). The occupancy of the phosphate group in the A and B chains was refined to 0.91 and 1.0, respectively. The anions are held in place by Zn_1 and charged hydrogen bonds to the guanidino nitrogen atoms of Arg166. One of the oxygen atoms of the phosphate group was 2.3 Å away from Zn_1 while the other two were 2.6 Å and 2.7 Å away from the guanidino nitrogen atoms of Arg166 (Table 5). The phosphate group moved 3.7 Å away from Zn_2 in the K328H structure relative to the wild-type structure, outward towards the solvent, and too far to be coordinated to Zn_2 (Table 5). In the wild-type structure the oxygen atom of the phosphate group is located 1.8 Å from Zn_2 (Figure 6). The average *B*-factor of the phosphate in the K328H structure was 72 Å^2 while in the wild-type structure it is about 20 Å^2.

The position of Arg166 in the K328H structure (Figure 5) did not change significantly from its observed position in the wild-type structure. The density around Arg166 showed that the side-chain is constrained to a well-defined position by Asp101 and Asp153 (*via* a water molecule), as it is in the wild-type structure (Kim & Wyckoff, 1991). The distance between OD1 of Asp101 and NH1 of Arg166 was 2.0 Å, while the distance between NE of

Table 5. Metal-ligand distances in the wild-type, K328H, D153H, and DM structures

Distance between			Distance (Å)			
			Wild-type	K328H	D153H	DM
Zn_1	His412	NE2	2.02	1.96	1.90	1.99
	His331	NE2	2.08	2.10	1.96	2.10
	Asp327	OD1	2.13	2.30	2.20	2.30
		OD2	2.42	2.30	2.40	2.10
	PO_4	O1	2.04	2.60	2.10	—
		O2	—	2.20	—	2.90
Zn_2	Ser102	OG	3.90	1.90	2.10	2.20
	Asp51	OD1	2.08	1.98	2.10	1.90
	Asp369	OD1	1.80	2.00	2.10	1.96
	His370	NE2	2.03	2.20	2.10	2.00
	PO_4	O2	2.10	—	2.00	—
Zn_3 / Mg	Asp51	OD2	2.02	2.10	1.80	1.80
	Asp322	OE2	2.10	2.20	1.90	1.85
	Thr155	HG1	2.10	1.90	2.30	2.20
	Asp / His153	ND1	4.00	3.20	1.90	2.00
	H_2O		1.98	2.40	—	—
	H_2O		1.95	2.60	—	—
	H_2O		2.18	—	—	—

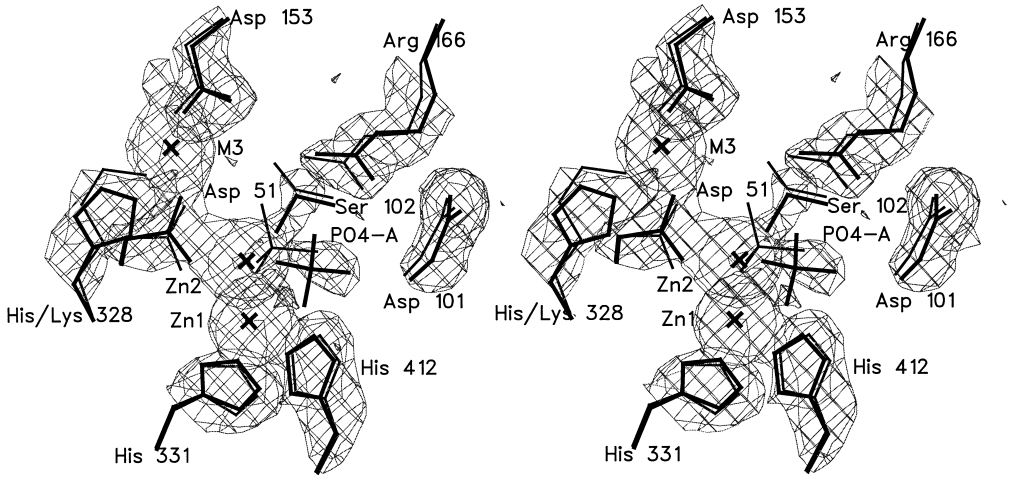

Figure 5. Stereoview showing the electron density of the active site of the K328H structure with the refined coordinates (thicker lines) overlaying the wild-type structure (thinner lines). The phosphate group (PO_4-A) in the K328H structure moved 2 Å from its position in the wild-type structure. Ser102 in the K328H structure is directly coordinated to zinc at the M2 binding site. Figures 5 through 8 were made using SETOR (Evans, 1993).

Arg166 and the oxygen atom of the water molecule coordinated to OD1 of Asp153 was 3.3 Å (Table 5).

A secondary anion binding site, previously reported in the structure of the D369N enzyme (Tibbitts *et al*., 1994), was observed in the K328H structure. In the crystals, this secondary anion binding site (PO_4-C) may be occupied by either a phosphate or sulfate group. In the K328H structure, the refined occupancy of the phosphate group at this site is 1.0 and 0.66 in the A and B chains, respectively.

The active site of the DM structure

The mutation of both Asp153 and Lys328 to histidine caused the loss of the salt-link existing between these two amino acid residues in the wild-type enzyme, as well as several other changes to the active site (Figure 7). The position of the imidazole side-chain of His328 was not precisely defined by the weak surrounding electron density, and the average temperature factor of His328 refined to about 50 $Å^2$. It was clear, however, that the density corresponded to a histidine and not a lysine side-chain due to the flattened ellipsoidal shape of the density, which was clearly not characteristic of a lysine side-chain. According to the electron density map, His328 appeared to adopt two alternative conformations. In one orientation the imidazole side-chain was pointed towards the active site, while in the other orientation His328 was pointed towards the solvent.

In the structure of the DM enzyme, the position

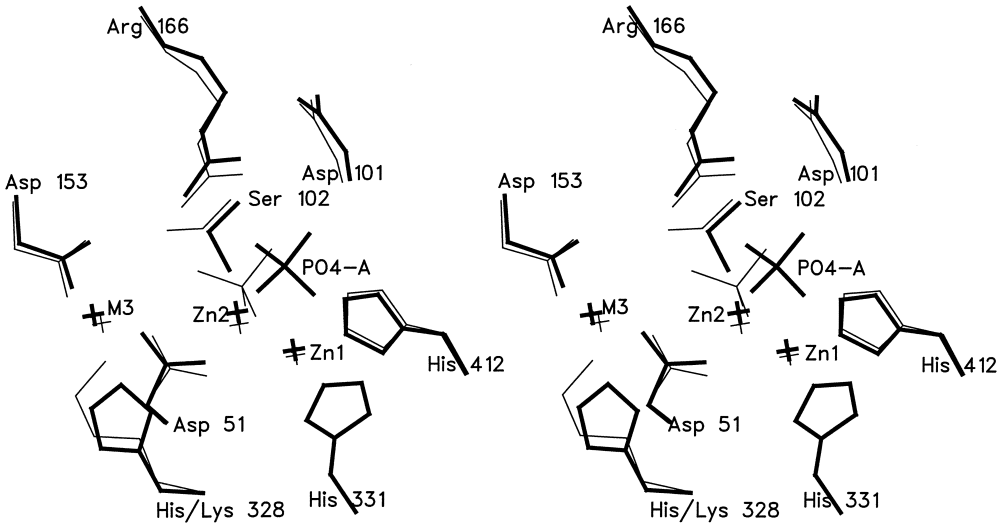

Figure 6. Stereoview comparing the active site ligands, metal ions and phosphate positions of the K328H mutant (thick lines) and the wild-type (thin lines). The phosphate group (PO_4-A) has moved out of the active site in the K328H mutant and is more exposed to the surface than in the wild-type. Ser102 has shifted and is coordinated to Zn_2 in the mutant structure.

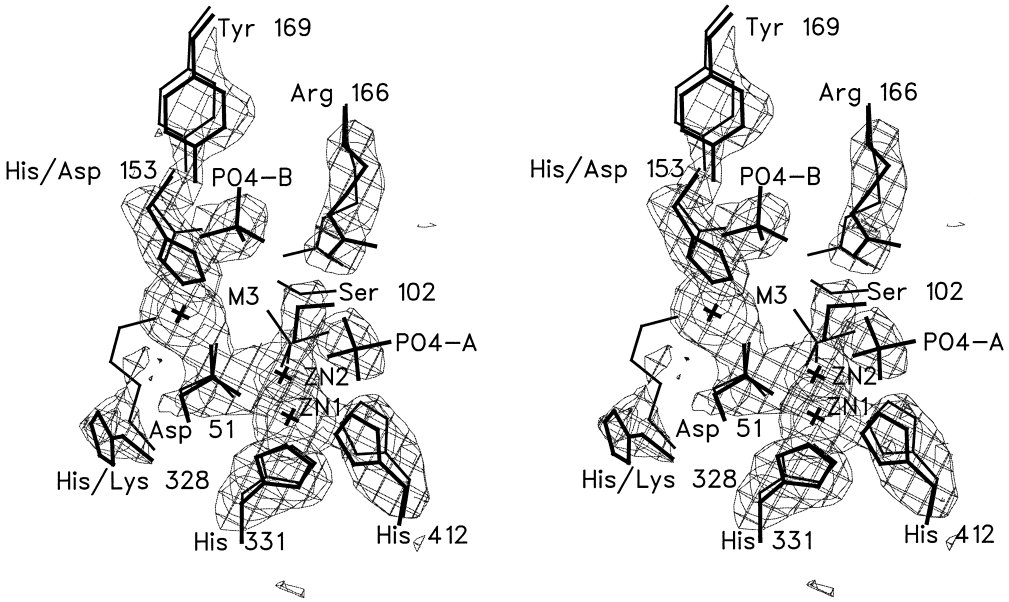

Figure 7. Stereoview showing the electron density of the active site, including the new anion binding site (PO_4-B) in the DM structure that is coordinated by Tyr169, Arg166 and His153. Water molecules are not shown in this figure. Note that the phosphate group (PO_4-A) has moved even further out of the active site than in the K328H structure. His153 has become a direct ligand to the metal ion at the M3 position. His328 is disordered as indicated by its omit density in this Figure. lt appears to be alternating between pointing towards the active site and towards the solvent.

of the phosphate group bound to the active site was dramatically different from both the wild-type and the K328H structures (Figure 8). In the DM structure the phosphate group moved 3.0 Å out of the active site towards the solvent, an even greater degree of displacement than was observed in the K328H structure (Table 5).

The X-ray structure of the DM enzyme (D153H / K328H) revealed an M3 metal site nearly identical with that previously reported for the D153H enzyme (Murphy & Kantrowitz, 1994; Murphy *et al*., 1993). The M3 site in the enzyme was occupied by a tetrahedrally coordinated zinc, replacing the octahedrally coordinated magnesium found in the wild-type structure (Figure 7). A number of observations suggested that the metal at the M3 site was not magnesium in the DM structure. First, after refinement with Mg^{2+} in the M3 site, the difference map ($F_o - F_c$) still showed considerable density at the position of the Mg^{2+}. Second, the temperature factors

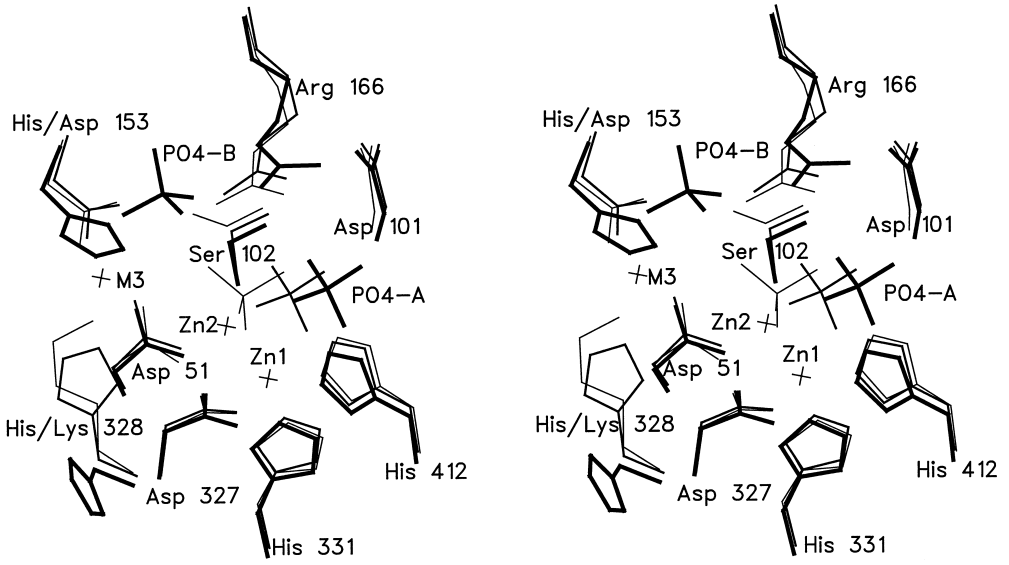

Figure 8. Stereoview comparing the three X-ray structures, wild-type (thinnest lines), K328H (middle lines) and DM (thickest lines). Note that His328 in the double mutant has flipped out, indicating its disorder. Also notice the three different positions of the phosphate group (PO_4-A) in all three structures. Ser102 is coordinated to Zn_2 in both mutant structures.

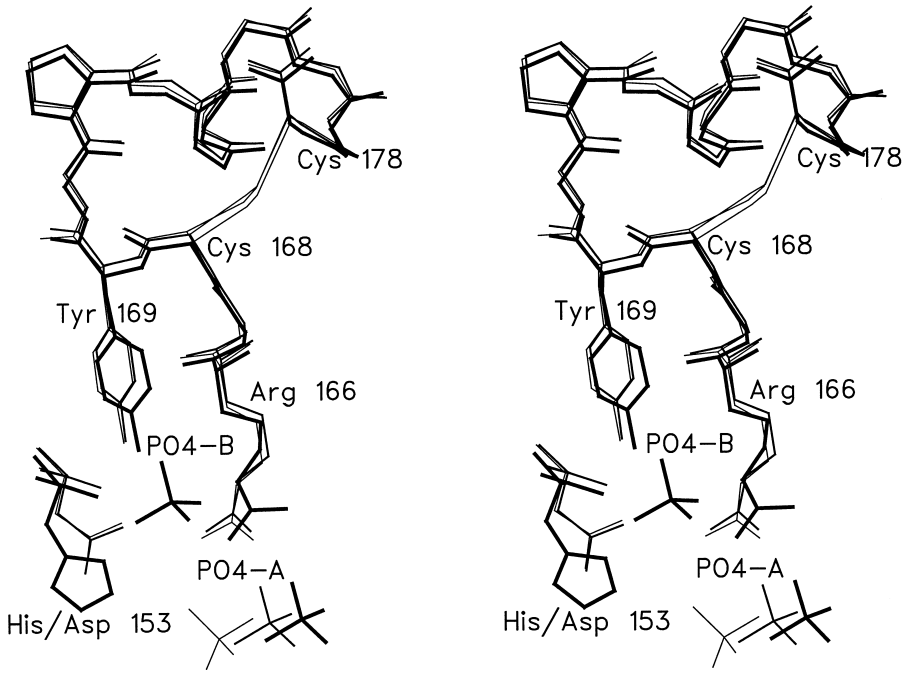

Figure 9. Stereoview comparing the wild-type (thinnest lines), the K328H (middle lines) and the DM (thickest lines) structures. This view focuses on the new anion binding site (PO_4-B) around Tyr169. This site exists in the D153H and DM structures, but is not seen in the K328H or the wild-type structure. The Figure shows the loop region formed by the disulfide bridge between Cys168 and Cys178. The conformation of this loop region appears to be conserved in all three structures.

of the Mg^{2+} atoms were significantly lower than the temperature factors of the atoms in the vicinity of the metal binding sites. Third, the difference map indicated that the only additional density in the coordination sphere of the Mg^{2+} was at the metal itself. The density expected to correspond to the three water ligands of the Mg^{2+} observed in the wild-type structure was not observed, suggesting that the metal coordination was not octahedral as expected for magnesium. Finally, the side-chain of His153 was close enough to be a direct ligand to the metal. Taken together, these observations indicated that the metal coordination had changed from octahedral to tetrahedral, somewhat unexpected for Mg^{2+}. Therefore, Zn^{2+} was modeled into the M3 site.

In the DM structure, Zn_1 is tetrahedrally coordinated by the NE2 nitrogen atoms of His412 and His331, OD1 and OD2 of Asp327 (which acts as a bidentate ligand), but not phosphate. In the wild-type structure, Zn_1 is coordinated to the phosphate group as well as the ligands mentioned above (Table 5). Zn_2 in the DM structure is similar to the K328H structure, being coordinated tetrahedrally by the hydroxyl group of Ser102, the OD1 oxygen atoms of Asp51 and Asp369, and NE2 of His370. In the wild-type structure Zn_2 is not coordinated to the hydroxyl group of Ser102, instead it is coordinated to the O_2 oxygen atom of the phosphate group (Figure 7).

Asp153 is thought to restrict the guanidino side-chain of Arg166, through a water-mediated interaction, to a position favorable for phosphate binding (Chen *et al*., 1992; Kim & Wyckoff, 1991). Since this interaction no longer exists in the DM structure, the substitution should result in destabilization of the position of Arg166. This was indicated by the greater hydrogen bond lengths between the NH1 and NH2 amino groups of Arg166 and the O3 and O4 oxygen atoms of the phosphate groups, which were 3.4 Å and 2.9 Å, respectively (Table 5).

The secondary anion binding site (PO_4-C) previously discussed was also observed in the DM structure (Tibbitts *et al*., 1994). The refined occupancy of this site was 0.88 in the A chain and 0.75 in the B chain. A new anion binding site (PO_4-B), first described here in the D153H structure, was also found in the DM structure (Figure 8 and 9). The anion, which may be a sulfate or phosphate group, is coordinated by the hydroxyl group of Tyr 169, two water molecules, and electrostatic interactions with NE of Arg166 and ND2 of His153, and had an occupancy of 0.74 in the A chain. Its position in the B chain was not clearly defined, although there was a broad area of density in omit maps near Tyr169. There was no evidence for this site in the K328H structure.

Discussion

The D153H, K328H and DM structures have zinc bound in all the metal sites

X-ray diffraction analysis of the D153H, K328H and DM crystals at pH 7.5 indicate that zinc is bound in all six metal sites. However, the metal occupancy, particularly at the M3 site, may be influenced

dramatically by the crystallization conditions. The presence of zinc and not magnesium at the M3 site agrees with the kinetic studies, which indicated that the D153H and DM enzymes have low activity under the crystallization conditions and are activated by magnesium. The K328H enzyme, though not activated by magnesium, has a lower affinity for magnesium than the wild-type enzyme (Janeway *et al*., 1993; Xu & Kantrowitz, 1991). Furthermore, kinetic studies on the D153H enzyme showed that zinc and magnesium compete for the same site on the enzyme (Murphy & Kantrowitz, 1994; Murphy *et al*., 1993). These results suggest that the human placental and yeast enzymes, as purified, may have zinc bound in the three metal binding sites, since these enzymes require the addition of magnesium for full activity (Cathala *et al*., 1975; Schurr & Yagil, 1971).

The coordination of zinc in the M3 site is tetrahedral, which is a more closely packed coordination sphere than the octahedral coordination of magnesium seen in the wild-type structure. When magnesium is bound at the M3 site in the wild-type structure, the octahedral coordination is more open and possibly less rigid than when zinc is bound in the D153H, K328H, and DM structures. Under high activity conditions, His153 may no longer be coordinated directly to the M3 site in the mutant structures, and magnesium in the M3 site may restore an octahedral coordination. This would leave the active site in a less rigid conformation, possibly more favorable for catalysis.

The salt-link between Asp153 and Lys328 is important for catalysis

The salt-link that exists between Asp153 and Lys328 in wild-type *E. coli* alkaline phosphatase previously shown to be important for phosphate binding (Janeway *et al*., 1993), no longer exists in the D153H, K328H and DM enzymes. The disruption of the salt-link increases the affinity of the D153H enzyme for phosphate compared with the wild-type enzyme (Janeway *et al*., 1993). The X-ray structure of the D153H enzyme shows that the side-chain of Lys328 repositions so that the ϵ-amino group can interact with the phosphate group, explaining the tighter phosphate binding observed for the D153H enzyme.

In the K328H structure, the phosphate group has shifted away from the catalytic pocket towards the solvent. The replacement of Lys328 by histidine eliminated the water-mediated interaction between Lys328 and phosphate observed in the wild-type structure. The displaced phosphate correlates well with the kinetic results, which showed a decrease in phosphate affinity as well as an increase in K_m and K_i for P_i (Janeway *et al*., 1993). The yeast enzyme, whose active site has histidine at position 328 and aspartate at position 153, has a 22-fold higher K_m and a substantially reduced affinity for phosphate compared with the *E. coli* enzyme (Schurr & Yagil, 1971; and see Table 2).

The DM structure was designed to more closely resemble the active site of the mammalian b/k/l, intestinal and placental enzymes, having histidine at positions 153 and 328. These substitutions, when combined, lead to an even further displacement of the phosphate group toward the solvent compared with the wild-type and the K328H structures. The movement of the phosphate even further towards the solvent in the DM structure could also be a result of the elimination of the water-mediated interactions between Asp153 and phosphate that exist in the wild-type structure (Kim & Wyckoff, 1991). The D153H enzyme has the lowest phosphate K_i value, followed by the wild-type, then the K328H, and finally the DM enzyme. This order of phosphate binding from tightest to weakest based on kinetic data (Table 2) is in agreement with the relative phosphate positions and the strength of its interactions with the protein in each of the *E. coli* structures (Figures 8 and 9).

The structural results agree with the pre-steady state kinetics, which are indicative of a change in the catalytic mechanism

Previous studies suggested that the rate-determining step of the D153H, K328H and DM enzymes changed from the release of phosphate from the non-covalent $E \cdot P_i$ complex to the hydrolysis of the $E\text{-}P_i$ covalent complex relative to the wild-type enzyme (Janeway *et al*., 1993; Xu & Kantrowitz, 1991). Our structural results further support these conclusions. The hydroxyl group of Ser102 in the D153H, K328H and DM structures directly interacts with Zn_2, similar to what is seen in the cadmium-substituted and the phosphate-free crystals of the wild-type enzyme (Kim & Wyckoff, 1991). The wild-type structure with phosphate bound resembles the non-covalent $E \cdot P_i$ complex, since Ser102 is not coordinated to Zn_2 or to the phosphate group. The displacement of the phosphate group in all three mutant structures may indicate that the phosphorylated substrate cannot bind correctly with zinc in the M3 site. Therefore, the phosphate group will not be in an optimal position for the nucleophilic attack that initiates catalysis. Since the formation of the serine-phosphate covalent intermediate may be hindered by the altered substrate binding, it becomes the rate-determining step, significantly slower than release of the phosphate product.

Altered substrate binding may not be the only factor effecting catalysis. The changes in the hydrogen-bonding network and the electrostatic potential in the active site caused by the loss of Asp153 and Lys328 in the D153H, K328H and DM enzymes could also influence catalysis. These changes could affect the protonation of the nucleophile activated in the first step of the reaction and thereby alter catalysis in the mutant enzymes leading to the observed shift in the pH *versus* activity profile.

Is the conversion of a water binding site to an anion binding site, by the introduction of histidine for aspartate at position 153, relevant to the human alkaline phosphatases?

The new anion site (PO_4-B) found in the double mutant and in the D153H mutant enzymes (Figure 9) provides some indications as to how these bacterial models may be related to the human enzymes, as well as some clues to the structural basis for the enhanced activity and lower thermal stability observed for the mammalian enzymes. The histidine substitution for aspartate at position 153 alters the net charge on the protein monomer by +2, which is expected to have a strong, fairly localized effect on the electrostatic potential in the space between residues His153, Tyr169 and Arg166. In the crystals at pH 7.5, zinc is at the M3 site, and His153 is constrained by zinc in such a way as to provide a hydrogen bond donor to an anion that may bind in this pocket. With tetrahedral zinc in the M3 site, there is additional space near Tyr169 and Arg166 that will accommodate a divalent anion, such as SO_4^{2-}, or HPO_4^{2-}, to exactly balance the charge locally, and should be favored over the binding of either water or OH^- at the side of the guanidino group of Arg166 that is observed in the *E. coli* wild-type enzyme.

As the pH is increased to more alkaline conditions, there will be a tendency for Tyr169 to ionize. If magnesium is provided, it can possibly replace zinc at the M3 site, and impose octahedral geometry, leaving a mostly uncharged histidine residue at position 153. The mutant protein will then have compensated for the additional +2 charges, and a OH^- or water molecule will be favored to occupy the site next to Arg166, as is the case in the wild-type structure at pH 7.5. This situation would explain the shift in the pH optimum observed for the D153H and DM enzymes.

If a similar situation exists in the mammalian systems, the shifted pH optimum of the mammalian enzymes may be due to inhibition by HPO_4^{2-}, binding to the anion binding site that we first discovered in the bacterial model enzymes. The higher pH may be needed so that Tyr169 is partially ionized to prevent binding of the anion. Thus the indicated role of Tyr169 in the mammalian systems would be to protect the flanking nitrogen atom of Arg166 from inhibition by phosphate and to ensure productive binding of the substrate.

Conclusion

The importance of Asp153 and Lys328 for magnesium and phosphate binding in *E. coli* alkaline phosphatase has been demonstrated by the D153H, K328H and DM structures. The structural results reported here suggest explanations for the activation by magnesium, the alterations in phosphate binding, the altered pH *versus* activity profiles, and the changes in the rate-determining step exhibited by the D153H, K328H and DM enzymes. The X-ray structures presented here of the *E. coli* enzymes, particularly in the active site region, may be similar to the active sites of the mammalian and yeast enzymes that have histidine at positions 153 and 328, since these residues are responsible for many of the observed kinetic differences between the bacterial, yeast and mammalian enzymes.

Methods

Materials

Agar, agarose, ampicillin, *p*-nitrophenyl phosphate, sodium dihydrogen phosphate, magnesium chloride and zinc chloride were purchased from Sigma Chemical Co. Tris, enzyme-grade ammonium sulfate, and sucrose were supplied by ICN Biomedicals. Tryptone and yeast extract were obtained from Difco Laboratories.

Strains

The Δ*phoA E. coli* K12 strain SM547 [Δ(*phoA-phoC*), *phoR*, tsx::Tn*5*, Δ*lac*, *galK*, *galU*, *leu*, *str*^{r}] was a gift from H. Inouye.

Expression and purification of the K328H and DM alkaline phosphatases

The K328H and DM enzymes were purified as reported previously (Janeway *et al*., 1993; Xu & Kantrowitz, 1991) using *E. coli* strain SM547 that had been transformed with plasmids pEK145 and pEK190, respectively. *E. coli* strain SM547 was used as the host strain for expression of the mutant enzymes because this strain contains a chromosomal deletion of the wild-type *phoA* gene and a mutation in the *phoR* regulatory gene. Therefore, no contamination from the wild-type alkaline phosphatase was possible.

Crystallization of K328H and DM enzymes

The K328H and DM enzymes were crystallized by vapor diffusion using hanging drops of 15 μl. The enzyme solution, at approximately 30 mg/ml, was first dialyzed against a 20% saturated solution of $(NH_4)_2SO_4$ in 100 mM Tris, 10 mM $MgCl_2$, 0.01 mM $ZnCl_2$ (pH 9.5). It took about two to three weeks for the crystals to form in reservoirs where the ammonium sulfate concentration was between 36 and 39% saturated. Before mounting in glass capillaries, the crystals were transferred into a stabilizing solution containing 65% saturated $(NH_4)_2SO_4$, 100 mM Tris, 10 mM $ZnCl_2$, 10 mM $MgCl_2$, 2 mM NaH_2PO_4 at pH 7.5 (Kim & Wyckoff, 1991).

X-ray data collection

The diffraction data were collected using one area detector (Area Detector Systems), driven by a MicroVAX 3500 computer and linked to a Rigaku RU-200 rotating-anode generator operated at 50 kV and 150 mA using the Crystallographic Facility in the Chemistry Department of Boston College. The instrumental setup has been described (Tibbitts *et al*., 1994). Diffraction data were collected to 2.16 Å and 2.38 Å respectively for the K328H and the DM crystals (Table 3). For the K328H structure, a total of 55,520 unique reflections were obtained from 214,

198 measurements with an average redundancy of 3.9 (Table 3). For the DM structure, of the 39,775 unique reflections, 118,201 were collected with an average redundancy of 3.0 (Table 3).

Merging of reflections was accomplished using the software provided by Area Detector Systems (Howard *et al*., 1985). After correction for Lorentz and polarization effects, a scale factor was calculated for multiple measurements and symmetry-related reflections. For each structure the diffraction data were merged and edited until R_{merge}† converged (Table 3).

Structural refinement

The progression of each structural refinement was monitored by the working *R*-factor, and the free *R*-factor, using cross-validation (Brünger, 1992a). The coordinates were refined for each mutant using the wild-type coordinates for *E. coli* alkaline phosphatase (Brookhaven Data Bank file 1ALK) as the initial model, with metal ions, phosphate group and water molecules removed. The sequence editing features of QUANTA (Molecular Simulations, Inc. Burlington, MA) were used to replace both Asp153 and Lys328 by histidine. X-PLOR v.3.1 (Brünger, 1992b) and IMPLOR (Polyvision, Inc. Hopedale, MA) were used to refine the coordinates. Positional refinement and temperature factor refinement improved the working and free *R*-factors and stereochemistry, initially. At this stage, the metal ions, their water ligands and the phosphate group were built in according to the calculated electron density ($2F_o - F_c$) and ($F_o - F_c$) maps, and simulated annealing omit maps (Brünger *et al*., 1990). The structures were further refined by positional refinement, temperature factor refinement, and simulated annealing using initial temperatures up to 3000°C. The refinements were carried out using the Silicon Graphics Indigo II computers at Boston College, and the Cray Y-MP C90 at the Pittsburgh Supercomputer Center. An automated water placement feature of IMPLOR was used to add solvent water molecules based on the difference Fourier map ($F_o - F_c$), their distance from surrounding residues, and their temperature factors. During the refinement non-crystallographic symmetry constraints (Tibbitts *et al*., 1994) were also imposed. For comparison the D153H structure was refined again using this method, and the previously obtained data (Murphy *et al*., 1993). The coordinates for the D153H, K328H and DM structures have been deposited in the Brookhaven Protein Data Bank as 2ANH, 1ANJ, and 1ANI, respectively.

Acknowledgements

This work was supported by grant GM42833 from the National Institute of General Medical Sciences and by Pittsburgh Supercomputing Center grant 1 P41 RR06009 from the NIH National Center for Research Resources. We thank H. W. Wyckoff and E. E. Kim for providing the X-ray coordinates of the wild-type enzyme prior to their deposition in the Brookhaven Protein Data Bank (1ALK).

$$\dagger\ R_{merge} = \frac{\sum_{hkl}\sum_{i} |I_{mean} - I_i|}{\sum_{hkl}\sum_{i} I_i}.$$

References

Anderson, R. A., Bosron, W. F., Kennedy, F. S. & Vallee, B. L. (1975). The role of magnesium in *Escherichia coli* alkaline phosphatase. *Proc. Natl Acad. Sci. USA*, **72**, 2989–2993.

Anderson, R. A., Kennedy, F. S. & Vallee, B. L. (1976). The effect of Mg(II) on the spectral properties of Co(II) alkaline phosphatase. *Biochemistry*, **15**, 3710–3715.

Berger, J., Garattini, E., Hua, J.-C. & Udenfriend, S. (1987). Cloning and sequencing of human intestinal alkaline phosphatase. *Proc. Natl Acad. Sci. USA*, **84**, 695–698.

Bloch, W. & Gorby, M. S. (1980). Catalytic mechanism of *Escherichia coli* alkaline phosphatase: resolution of three variants of the acyl-enzyme mechanism. *Biochemistry*, **19**, 5008–5018.

Bradshaw, R. A., Cancedda, F., Ericsson, L. H., Newman, P. A., Piccoli, S. P., Schlesinger, K. & Walsh, K. A. (1981). Amino acid sequence of *Escherichia coli* alkaline phosphatase. *Proc. Natl Acad. Sci. USA*, **78**, 3473–3477.

Brändén, C.-I. & Jones, T. A. (1990). Between objectivity and subjectivity. *Nature*, **343**, 687–689.

Brooks, B. R., Bruccoleri, R. E., Olafson, B. D., States, D. J., Swaminathan, S. & Karplus, M. (1983). CHARMM: a program for macromolecular energy, minimization, and molecular dynamics calculations. *J. Comput. Chem.* **4**, 187–217.

Brunel, C. & Cathala, G. (1973). Activation and inhibition processes of alkaline phosphatase from bovine brain by metal ions (Mg^{2+} and Zn^{2+}). *Biochim. Biophys. Acta*, **309**, 104–115.

Brünger, A. T. (1992a). Free R value: a novel statistical quantity for assessing the accuracy of crystal structures. *Nature*, **355**, 472–475.

Brünger, A. T. (1992b). *X-PLOR, Version 3.1*, Yale University Press, New Haven, CT.

Brünger, A. T. (1993). Assessment of phase accuracy by cross validation: the free R value. Methods and applications. *Acta Crystallog. sect. D*, **49**, 24–36.

Brünger, A. T., Krukowski, A. & Erickson, J. W. (1990). Slow-cooling protocols for crystallographic refinement by simulated annealing. *Acta Crystallog. sect. A*, **46**, 585–593.

Cathala, G., Brunel, C., Chappelet-Tordo, D. & Lazdunski, M. (1975). Bovine kidney alkaline phosphatase. Catalytic properties, subunit interactions in the catalytic process, and mechanism of Mg^{2+} stimulation. *J. Biol. Chem.* **250**, 6046–6053.

Chen, L., Neidhart, D., Kohlbrenner, M., Mandecki, W., Bell, S., Sowadski, J. & Abad-Zapatero, C. (1992). Three-dimensional structure of a mutant (Asp101 → Ser) of alkaline phosphatase with higher catalytic efficiency. *Protein Eng.* **5**, 605–610.

Coleman, J. (1992). Structure and mechanism of alkaline phosphatase. *Annu. Rev. Biophys. Biomol. Struct.* **21**, 441–483.

Engh, R. A. & Huber, R. (1991). Accurate bond and angle parameters for X-ray protein structure refinement. *Acta Crystallog. sect. A*, **47**, 392–400.

Evans, S. (1993). SETOR: Hardware-lighted three-dimensional solid representations of macromolecules. *J. Mol. Graphics*, **11**, 134–138.

Gettins, P. & Coleman, J. E. (1983). ^{31}P nuclear magnetic resonance of phosphoenzyme intermediates of alkaline phosphatase. *J. Biol. Chem.* **258**, 408–416.

Harkness, D. R. (1968). Studies on human placental alkaline phosphatase. II. Kinetic properties and

studies on the apoenzyme. *Arch. Biochem. Biophys.* **126**, 513.

Hodel, A. (1992). Model bias in macromolecular crystal structures. *Acta Crystallog. sect. A*, **48**, 851–858.

Howard, A. J., Nielsen, C. & Xuong, N. H. (1985). Software for a diffractometer with multiwire area detector. *Methods Enzymol.* **114**, 452–471.

Hua, J.-C., Berger, J., Pan, Y.-C. E., Hulmes, J. D. & Udenfriend, S. (1986). Partial sequencing of human adult, human fetal, and bovine intestinal alkaline phosphatases: comparison with the human placental and liver isozymes. *Proc. Natl Acad. Sci. USA*, **83**, 2368–2372.

Hull, W. E., Halford, S. E., Gutfreund, H. & Sykes, B. D. (1976). ^{31}P nuclear magnetic resonance study of alkaline phosphatase: the role of inorganic phosphate in limiting the enzyme turnover rate at alkaline pH. *Biochemistry*, **15**, 1547–1561.

Janeway, C. M. L., Xu, X., Murphy, J. E., Chaidaroglou, A. & Kantrowitz, E. R. (1993). Magnesium in the active site of *Escherichia coli* alkaline phosphatase is important for both structural stabilization and catalysis. *Biochemistry*, **32**, 1601–1609.

Kam, W., Clauser, E., Kim, Y. S., Kan, Y. W. & Rutter, W. J. (1985). Cloning, sequencing, and chromosomal localization of human term placental alkaline phosphatase. *Proc. Natl Acad. Sci. USA*, **82**, 8715–8719.

Kaneko, Y., Hayashi, N., Toh-e, A., Banno, I. & Oshima, Y. (1987). Structural characteristics of the PHO8 gene encoding repressible alkaline phosphatase in *Saccharomyces cerevisiae*. *Gene*, **58**, 137–148.

Kim, E. E. & Wyckoff, H. W. (1991). Reaction mechanism of alkaline phosphatase based on crystal structures. *J. Mol. Biol.* **218**, 449–464.

Laskowski, R. A., MacArthur, M. W., Moss, D. S. & Thornton, J. M. (1993). PROCHECK: a program to check the stereochemical quality of protein structures. *J. Appl. Crystallog.* **26**, 283–291.

Luzzati, P. V. (1952). Traitement statistique des erreurs dans la determination des structures Cristallines. *Acta Crystallog.* **5**, 802–810.

Ma, L., Tibbitts, T. T. & Kantrowitz, E. R. (1995). *Escherichia coli* alkaline phosphatase: X-ray structural studies of a mutant enzyme (His-412 → Asn) at one of the catalytically important zinc binding sites. *Protein Sci*. **4**, 1498–1506.

Murphy, J. E. & Kantrowitz, E. R. (1994). Why are mammalian alkaline phosphatases much more active than bacterial alkaline phosphatases? *Mol. Microbiol.* **12**, 351–357.

Murphy, J. E., Xu, X. & Kantrowitz, E. R. (1993). Conversion of a magnesium binding site into a zinc binding site by a single amino acid substitution in *Escherichia coli* alkaline phosphatase. *J. Biol. Chem.* **268**, 21497–21500.

Reid, T. W. & Wilson, I. B. (1971). *E. coli* alkaline phosphatase. *Enzymes* (Boyer, P. D., ed.), 3rd edit., vol. 4, pp. 373–415, Academic Press, New York.

Schurr, A. & Yagil, E. (1971). Regulation and characterization of acid and alkaline phosphatase in yeast. *J. Gen. Microbiol.* **65**, 291–303.

Schwartz, J. H. & Lipmann, F. (1961). Phosphate incorporation into alkaline phosphatase of *E. coli*. *Proc. Natl Acad. Sci. USA*, **47**, 1996–2005.

Sowadski, J. M., Handschumacher, M. D., Murthy, H. M. K., Kundrot, C. & Wyckoff, H. W. (1983). Crystallographic observations of the metal ion triple in the active site of alkaline phosphatase. *J. Mol. Biol.* **170**, 575–581.

Sowadski, J. M., Handschumacher, M. D., Murthy, H. M. K., Foster, B. A. & Wyckoff, H. W. (1985). Refined structure of alkaline phosphatase from *Escherichia coli* at 2.8 Å resolution. *J. Mol. Biol.* **186**, 417–433.

Tibbitts, T. T., Xu, X. & Kantrowitz, E. R. (1994). Kinetics and crystal structure of a mutant *Escherichia coli* alkaline phosphatase (Asp-369 → Asn): a mechanism involving one zinc per active site. *Protein Sci.* **3**, 2005–2014.

Weiss, M. J., Henthorn, P. S., Lafferty, M. A., Slaughter, C., Raducha, M. & Harris, H. (1986). Isolation and characterization of a cDNA encoding a human liver/bone/kidney-type alkaline phosphatase. *Proc. Natl Acad. Sci. USA*, **83**, 7182–7186.

Xu, X. & Kantrowitz, E. R. (1991). A water-mediated salt link in the catalytic site of *Escherichia coli* alkaline phosphatase may influence activity. *Biochemistry*, **30**, 7789–7796.

Edited by T. Richmond

(Received 7 June 1995; accepted 11 August 1995)